Tellus SERIES B CHEMICAL AND PHYSICAL METEOROLOGY
PUBLISHED BY THE INTERNATIONAL METEOROLOGICAL INSTITUTE IN STOCKHOLM

Tellus (2010)

TELLUS

Simulation studies for a space-based CO_2 lidar mission

By S. R. KAWA[1]*, J. MAO[2], J. B. ABSHIRE[1], G. J. COLLATZ[1], X. SUN[1] and C. J. WEAVER[2],
[1]*NASA Goddard Space Flight Center, Greenbelt, MD, USA;* [2]*Goddard Earth Sciences and Technology Center, University of Maryland Baltimore County, Baltimore, MD, USA*

(Manuscript received 22 December 2009; in final form 25 June 2010)

ABSTRACT

We report results of initial space mission simulation studies for a laser-based, atmospheric CO_2 sounder, which are based on real-time carbon cycle process modelling and data analysis. The mission concept corresponds to the Active Sensing of CO_2 Emissions over Nights, Days and Seasons (ASCENDS) recommended by the US National Academy of Sciences' Decadal Survey. As a pre-requisite for meaningful quantitative evaluation, we employ a CO_2 model that has representative spatial and temporal gradients across a wide range of scales. In addition, a relatively complete description of the atmospheric and surface state is obtained from meteorological data assimilation and satellite measurements. We use radiative transfer calculations, an instrument model with representative errors and a simple retrieval approach to quantify errors in 'measured' CO_2 distributions, which are a function of mission and instrument design specifications along with the atmospheric/surface state. Uncertainty estimates based on the current instrument design point indicate that a CO_2 laser sounder can provide data consistent with ASCENDS requirements and will significantly enhance our ability to address carbon cycle science questions. Test of a dawn/dusk orbit deployment, however, shows that diurnal differences in CO_2 column abundance, indicative of plant photosynthesis and respiration fluxes, will be difficult to detect.

1. Introduction

Carbon dioxide (CO_2) is the largest known anthropogenic forcing of climate change, yet substantial uncertainty is attached to the current atmospheric CO_2 budget. Global, decadal budgets infer a large residual sink for atmospheric CO_2 with attached uncertainty of 50–100% or more (IPCC, 2007; SOCCR, 2007). Several lines of evidence suggest that the Northern Hemisphere terrestrial biosphere is responsible, but the magnitude, location and mechanisms producing the sink are not well determined (Tans et al., 1990; Bousquet et al., 2000; Stephens et al., 2007). Furthermore, interannual variability in the increase of atmospheric CO_2, and hence variation in the terrestrial sink (and to a lesser extent ocean), is large, but the forcing/response mechanisms and connection to decadal processes are not quantitatively resolved (Langenfelds et al., 2002; Nemani et al., 2003; Baker et al., 2006). As a result, carbon–climate interaction is among the leading sources of uncertainty in prediction of future climate (Cox et al., 2000; Dufresne et al., 2002, Friedlingstein et al., 2006). To a large extent, our ability to quantify CO_2 sources and sinks using diagnostic models is hampered by sparse data limitations (Gurney et al., 2002).

New global remote sensing data from satellites hold great promise to reduce CO_2 source/sink uncertainties (e.g. Rayner and O'Brien, 2001). The CO_2 measurement precision and accuracy requirements, however, are unprecedented for atmospheric constituents from space. High precision, dedicated measurements of CO_2 from space are just now becoming available from the Greenhouse gases Observing SATellite (GOSAT aka IBUKI) (Yokota et al., 2004). GOSAT, and those planned from the Orbiting Carbon Observatory (OCO) (Crisp et al., 2004), uses passive spectroscopy of reflected near-infrared sunlight to retrieve total column CO_2 abundances. Passive instruments such as these, however, have inherent sampling limitations related to sun angle, surface reflectance and cloud cover (Miller et al., 2007; Chevallier et al., 2009). In addition, potential errors resulting from uncertainty in the impact of cloud and aerosol scattering can be significant (Dufour and Breon, 2003; Mao and Kawa, 2004).

Many of the shortcomings of passive CO_2 detection can be overcome with active CO_2 lidar measurements. For this reason, the US National Academy of Sciences Decadal Survey of Earth Science and Applications from Space recommended the Active Sensing of CO_2 Emissions over Nights, Days and Seasons (ASCENDS) mission for NASA launch in about 2016 (NRC, 2007). The key characteristics of ASCENDS would be highly precise global CO_2 measurements without seasonal, latitudinal or diurnal bias. The target precision for measuring CO_2

*Corresponding author.
e-mail: stephan.r.kawa@nasa.gov
DOI: 10.1111/j.1600-0889.2010.00486.x

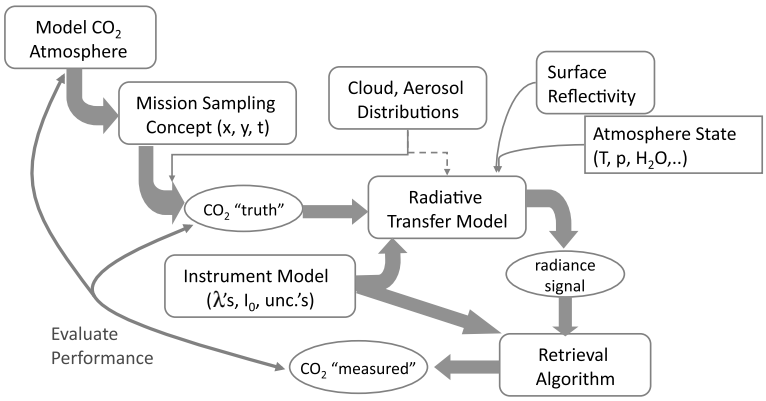

Fig. 1. Schematic diagram of the model framework to test performance and design options for a future CO_2 space mission. Flux inversion can be part of the 'evaluate' process.

is 0.5% at 100–200 km spatial scales over land and ocean, respectively, leading to surface flux quantification on 1° grids at weekly time resolution. Analysis of possible lidar techniques and performance indicates that such sensors are feasible (Menzies and Tratt, 2003; Ehret et al., 2008). Both ground-based and airborne CO_2 measuring lidar have been developed and demonstrated (see Dobbs et al., 2002; Koch et al., 2004; Gibert et al., 2006; Abshire et al., 2007, 2009; Kameyama et al., 2009).

In this paper, we present a modelling and data analysis framework developed to test the ability of a prospective lidar mission to measure known (modelled) atmospheric CO_2 distributions, to calculate the uncertainties associated with the measurements and to examine the sensitivity of the 'measured' CO_2 distributions and errors to varying environmental, mission and instrument design parameters. Figure 1 shows a schematic of the mission simulation process. Our approach is to constrain the simulation as closely as possible to real-world conditions using analysed meteorological fields, a model CO_2 atmosphere that represents observed gradients across a wide range of spatial/temporal scales, and collocated, contemporaneous observations of key environmental state variables. Because the CO_2 fluxes and transport are driven by real-time analysed weather fields, meteorologically driven covariances (e.g. synoptic weather–cloudiness–vegetation flux–CO_2 transport) and attendant potential biases are explicitly included in the simulations. The methodology is generally applicable to other measurement approaches including passive sensors.

The instrument radiance detection errors are derived from radiative transfer calculations and an instrument model that has been developed for the ASCENDS CO_2 lidar (Abshire et al., 2007). We use the resulting pseudo-data fields to estimate the performance of the current instrument design point in measuring global column CO_2 and to explore how this performance scales with several instrument and mission design options. We also use the pseudo data to address questions of how best to aggregate data to minimize uncertainties and maximize information content for carbon cycle science applications including a dawn/dusk versus midday/midnight orbit. Here, we use forward simulations to test the sensitivity of the inferred CO_2 distributions to design parameters for the CO_2 sounder concept. In the future, we plan to use an inverse model to evaluate the impacts on inferring surface sources and sinks of CO_2 (e.g. Rayner et al., 2002).

2. CO_2 flux and transport modelling

The CO_2 fields used for the simulation are taken from an updated version of the atmospheric flux and transport modelling of Kawa et al. (2004). Real-time, analysed meteorological fields from the Goddard Global Modelling and Assimilation Office, version GEOS-4, are used to drive both the biospheric flux and CO_2 transport models. Monthly global biosphere fluxes at $1^\circ \times 1^\circ$ are produced from the Carnegie-Ames-Stanford Approach (CASA) model using mean GEOS-4 meteorology and monthly Normalized Difference Vegetation Index (NDVI) data (Tucker et al., 2005). Three-hourly net ecosystem exchange and respiration are generated from the monthly values using 3-h GEOS-4 radiation and temperature in the method of Olsen and Randerson (2004). Biomass burning from GFED2 (van der Werf et al., 2006) is included in the CASA monthly fluxes. Fossil fuel and ocean fluxes are adopted from TransCom-C (Law et al., 2008). The transport model grid used here is $1^\circ \times 1.25^\circ \times 28$ levels with output hourly. The model CO_2 output has been extensively compared to *in situ* and remote sensing observations at a wide variety of sites. In most cases, the model simulates diurnal to synoptic to seasonal variability with a high degree of fidelity (Kawa et al., 2004; Bian et al., 2006; Law et al., 2008; Parazoo et al., 2008).

3. Orbit sampling

We use CALIPSO data (Winker et al., 2007) as the model for the CO_2 laser sounder orbital sampling. CALIPSO travels in the so-called 'A-train' orbit, which is a 705-km sun-synchronous polar orbit with an equator-crossing time of about 1:30 a.m./p.m. local solar time, and a 16-day repeat cycle. The orbit inclination of 98.2° provides global coverage between 82°N and 82°S. The 5-km CALIPSO orbit data are sampled according to the nominal averaging time of the CO_2 laser sounder, 10 s in this case. This

produces samples approximately every 70 km along the orbit, which is a reasonable match to the resolution of the global CO_2 model. Model CO_2 profiles at the nearest output time are interpolated to the sample locations along with temperature and water vapour from the assimilation data for input to the radiative transfer calculations.

Surface reflectivity over land is interpolated from MODIS (Terra + Aqua) 5-km, 16-d composite nadir BRDF-adjusted reflectance data at 1.64 μm (band 6), which are available every 8 days (Schaaf et al., 2002). Recent analysis of POLDER, MODIS and expected lidar 'hot spot' reflectivity (Disney et al., 2009) suggests that the 1.64-μm nadir reflectance product should be reasonably accurate for the laser wavelengths (1572 nm) used here; a decrease in reflectance of 15–20% in going from 1.64 to 1.57 μm is compensated for by an enhancement factor of similar magnitude in viewing the nadir hot spot within 2°. Over ocean, nadir glint reflectance is calculated from GEOS-4 10-m wind speeds (Lancaster et al., 2005). Figure 2 shows the global surface reflectance for 2006-07-26 (using the MODIS composite from 2006-07-28 over land) and that interpolated to the orbit track for the day. Because the laser return signal is inversely proportional to reflectivity, the measurement uncertainty depends strongly on this variable, which varies widely around the globe (Fig. 2b). Reflectivity at these wavelengths is generally lower over ice and water than land, but the difference for the laser sounder is not as large as for passive sensors since the lidar continually views the glint point at nadir.

Extinction of the laser signal by clouds and aerosols is derived from CALIPSO measured optical depths. We use the CALIPSO level-2, version 2.01 cloud and aerosol optical depth profile products, which are reported every 5-km along track (see http://eosweb.larc.nasa.gov/PRODOCS/calipso/Quality_Summaries/CALIOP_L2LayerProducts_2.01.html). Although this is a beta CALIPSO product with known large uncertainties, we feel its use is justified because we only use the data at relatively low optical depths where the retrieval is best constrained, and because the data closely represent the cloud and aerosol distributions that the CO_2 laser would encounter. Cloud optical depths are reported for the 532 nm laser only presuming that cloud extinction is largely independent of wavelength. Aerosol optical depths are reported at 532 and 1064 nm. We use the 1064 nm product for completeness, but for our application the contribution of aerosol to the total attenuation is nearly negligible. Up to 10 layer optical depths are reported for each profile. We simply sum them all in the vertical to obtain a total cloud+aerosol optical depth (τ_c). This method underestimates actual optical depth in opaque clouds, but we only use the data in thin cloud/aerosol cases. Profile samples with τ_c greater than 1.0 are masked out in this analysis. The cut-off value of $\tau_c = 1.0$ was chosen as a qualitative compromise between minimizing the random error produced at high optical depth (low SNR) and maximizing the number of accepted samples. We examined use of a cut-off from 0.1 to 1.6 and selected

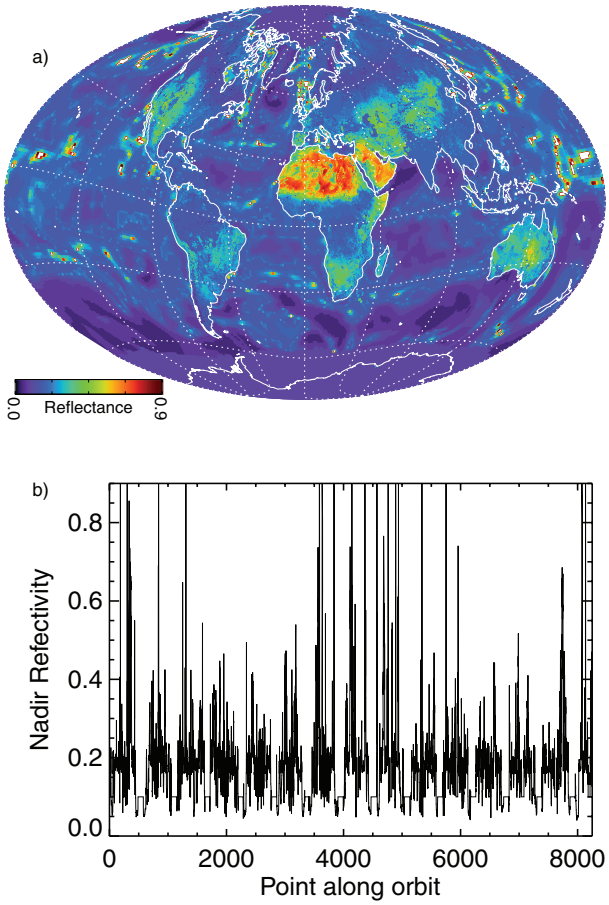

Fig. 2. Surface reflectance fraction used in the instrument performance simulations: (a) global and (b) sampled along the orbit track for one example day. Reflectance over land is obtained from the MODIS Band 6 16-d composite BRDF-adjusted nadir reflectance product. Missing data are filled with values of 0.2. Over water, Fresnel reflectance is calculated at nadir using 10-m wind speed from the meteorological analysis. Reflectance over ice that is not available from MODIS (e.g. in the polar dark) is assumed to be 0.1 (Warren, 1982). Ice cover extent is determined from the GEOS-4 analysis.

1.0 for the optimum ratio of sample number to SNR. This number will be optimized for the space instrument depending on actual performance. We decided to sample the CALIPSO 5-km fields rather than average along-track to represent optical depth for our 10-s (70-km) CO_2 sample profiles to retain the full probability distribution (PDF) of total optical depth. The τ_c data are highly variable so along-track averaging narrows the PDF (fewer high and low values), which results in fewer accepted samples at a given τ_c cutoff and thus greater overall CO_2 measurement uncertainty. We do not, however, expect the CO_2 space instrument to operate in a simple time averaging mode. Cloud-clearing will likely be done at a sample frequency greater than 1 Hz (roughly equivalent to the 5-km CALIPSO granule), producing a conditionally sampled average measurement with optical depth significantly less than the 10-s average.

For the dawn/dusk orbit test shown below, we shift the CALIPSO orbit points in time to a 0600/1800 hours equator crossing and sample the CO_2 and meteorological fields accordingly. CALIPSO cloud and aerosol fields are used as measured. Note also that the baseline radiance error calculations below are done for a 450-km orbit height, which is not fully consistent with the CALIPSO track, but this approximation will not significantly affect the sensitivity and uncertainty results.

4. Radiative transfer

For each orbit sample point, spectral atmospheric transmission for the laser target CO_2 line is calculated from the model sampled profiles (P, T, CO_2, H_2O) using the Line-By-Line Radiative Transfer Model (Clough et al., 1992; Clough and Iacono, 1995) and the HIgh-resolution TRANsmission molecular absorption (HITRAN) database 2008 version (Rothman et al., 2009). The measured cloud and aerosol optical depths are not explicitly included in the transmission calculations, but the transmission at all wavelengths in the CO_2 band centred at 1575 nm is diminished by a factor of EXP(-τ_c) (Fig. 3a). As stated earlier, only profiles with total cloud and aerosol optical depth less than 1.0 are retained for further analysis. In the test cases for July and December, 2006, this results in about 37–40% of the profiles being used. Retrievals from cloud top reflection may be possible in some cases, but we neglect those opportunities for now. Most variability in Fig. 3(a) results from cloud attenuation; aerosol optical depths are relatively small. Although cloud optical depths will in general be somewhat wavelength dependent, that difference between the CO_2 laser and CALIPSO wavelengths is expected to be about 30% (Warren, 1984), which is comparable to the overall uncertainty in measured τ_c.

5. Instrument and error model

The measurement radiance error model is based on the CO_2 laser sounder approach developed at NASA Goddard Space Flight Center (GSFC) for ASCENDS (Abshire at al., 2007). The technique is integrated path differential absorption laser spectroscopy. The space instrument concept uses several tunable fibre laser transmitters for simultaneous measurement of the absorption from a CO_2 line in the 1575 nm band, O_2 extinction in the oxygen A-band, and surface height and aerosol backscatter in the same path. One tunable laser is stepped across a single line for the CO_2 column measurement, whereas another laser is stepped across a pair of lines near 765 nm for the O_2 measurement (Stephen et al., 2007). The instrument directs the narrow, co-aligned laser beams toward nadir, and measures the energy of the laser echoes reflected from land and water surfaces. Narrow-linewidth lasers are stepped across the selected bands at a frequency of ~8 kHz. The receiver uses a 1.5-m-diameter telescope and photon counting detectors (Table 1). The detected signal includes background light and laser echoes from the surface along with scattering from any clouds or aerosols in the path. After suitable averaging the gas extinction and column densities for CO_2 and O_2 are estimated via differential absorption lidar (DIAL) techniques.

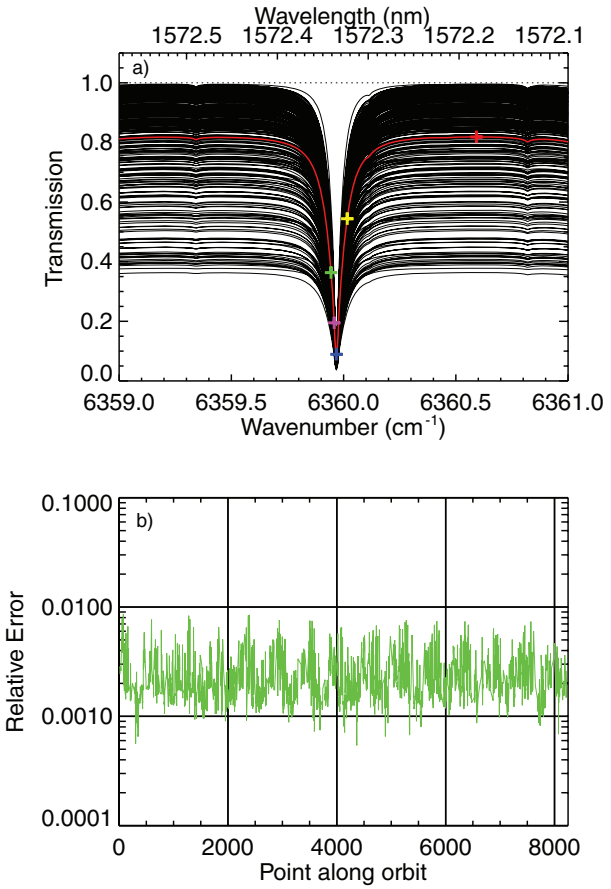

Fig. 3. Transmission (one-way) calculated for each profile sample of the 2007-07-26 test case [black lines, panel (a)] and relative error in on-line/off-line radiance detection (b). Wavelength-independent attenuation derived from observed CALIPSO cloud plus aerosol optical depth is applied to each profile. Average spectrum (red line) and candidate laser measurement wavelengths (plus symbols) are shown in colours. Transmission calculations are done at a wavenumber resolution of 0.002 cm^{-1} ($\Delta\lambda \sim 0.5$ pm). Samples with total optical depth >1.0 are screened from analysis (~37% accepted).

The CO_2 sounder approach uses pulsed lasers, a photon counting receiver, and time gating in the receiver to time (height) resolve the laser backscatter profile (Table 1). This allows signal processing to isolate the arrival time and energy in the laser return from the Earth's surface, and to exclude laser photons scattered from clouds and aerosols that generally arrive earlier. Hence, the technique allows isolating the full column CO_2 measurement from potential bias errors caused by atmospheric scattering, which is major advantage of this technique. Time gating centred around the ground echo pulse also substantially reduces solar background noise. Recent airborne experiments

Table 1. Lidar instrument model specifications

Design parameter	Value
Orbital altitude (km)	450
Laser peak power (W)	3000
Laser pulse width (μs)	1
Laser pulse rate (each wavelength) (Hz)	1200
CO_2 line centre wavelength (nm)	1572.33
Receiver telescope diameter (m)	1.5
Telescope and receiver transmission	0.45
Receiver optical bandwidth (nm)	0.4
Detector photon counting efficiency (%)	15
Detector dark count rate (Hz)	5×10^5
Measurement integration time (s)	10

show that with 1-μs transmitter pulses, the height of the laser reflecting layers, and hence the length of atmospheric path, can be determined to about 4 m.

Table 1 lists key instrument design parameters used to calculate the laser radiance random measurement errors. The lidar configuration and error model are similar to that evaluated by Ehret et al. (2008), and the sensitivities to atmospheric and instrument variables (e.g. telescope size, transmitter energy, detector efficiency) are generally the same. For a given instrument design the returned pulse power, and hence signal-to-noise ratio (SNR), depends most strongly on the atmospheric transmission and surface reflectivity. These values are drawn from the model samples, measurements and radiative transfer calculations as discussed earlier. The contribution of solar irradiance background noise is computed from the solar zenith angle at the sample point and the instrument optical parameters. The random relative error in the on-line/off-line radiance ratio (more below) for each profile of one test day is shown in Fig. 3(b). Random error varies by more than a factor of 10 among profiles around the globe depending on the atmospheric state. The root mean square (RMS) error is 0.0024, which corresponds to about 0.9 ppmv on a global background CO_2 of 375 ppmv. Calculations can be done at this level for any variety of instrument/mission specifications (as listed in Table 1) to determine the global sensitivity of the random error to these design choices. In general, the global mean error calculated in this way for a given instrument design is substantially different (larger) than that calculated using a global mean reflectance and/or uniform transmission estimate.

An additional error source of ± 2 mbar (uncorrelated with radiance error) is imposed for the surface pressure uncertainty in converting column CO_2 density to column average mixing ratio ($<CO_2>$). It is expected that surface pressure data will be available with this uncertainty either from the collocated laser measurements of O_2 column or from weather data assimilation. Additional errors induced by uncertainty in atmospheric variables (T, H_2O, aerosol) are expected to be small relative to a surface pressure error of this magnitude (Ehret et al., 2008). We include a 0.05% 'representation error' globally to account for the ability of the narrow ($\sim$70 m wide) laser sample stripe to measure mean $<CO_2>$ in a grid sample volume of about (70 km)^2 (Miller et al., 2007; Corbin et al., 2008). Another 0.1% uncorrelated error is introduced over land surfaces to account for noise produced by changes in surface reflectance and non-simultaneity of the laser footprints at the pulsed laser sample wavelengths (Amediek et al., 2009) along with other pointing/timing errors (Ehret et al., 2008). We have not included spectroscopy, a priori and retrieval fitting, or other systematic instrument errors at this time.

6. Simplified retrieval algorithm

For this work, we use a notional DIAL retrieval algorithm, which assumes that the sampled CO_2 column density is proportional to the logarithm of the on-line/off-line transmission ratio at selected wavelength points. The off-line wavelength is chosen to be where the sample-average absorption in the band is the minimum (Fig. 3a, red symbol). For on-line, we use the wavelength at which the average absorption is 50% (Fig. 3a, green symbol). The CO_2 error is then proportional to the relative uncertainty in the log of the on-line/off-line radiance ratio measurement, which is a function of the SNR at these wavelengths (e.g. Ehret et al., 2008). In the two-wavelength case, the relative error is the minimum for 50% absorption. In practice, an optimization algorithm using laser absorption at several wavelengths along the absorption line can be used to retrieve CO_2 column with varying vertical weighting functions. The current GSFC design allows for up to eight sample wavelengths distributed across the line. Measurement using multiple wavelengths also allows for reducing possible instrumental effects and more tightly controlling potential bias errors. The simple retrieval assumption used here can be viewed as a minimum-capability instrument case. The method is, however, quantitative for estimating the relative CO_2 measurement uncertainty and its sensitivity to changing conditions and instrument design parameters.

A uniform vertical weighting function is used to extract total column CO_2 from the model. Again, depending on the lidar design, a CO_2 vertical weighting function with multiple degrees of freedom will likely be possible with multiple laser wavelengths. This will result in improved sensitivity to variations of CO_2 in the lower atmosphere, which occur in response to surface sources and sinks—the ultimate objective of ASCENDS. For the cases studied here, we use error in total column as a conservative metric for the measurement error. Note that different weighting functions are simple to apply in the modelling framework and these can be tested in future studies.

7. Design point data error estimate

Figure 4(a) shows the full model $<CO_2>$ field at midday on 2006-07-26. Gradients of several ppmv/1000 km are seen in the

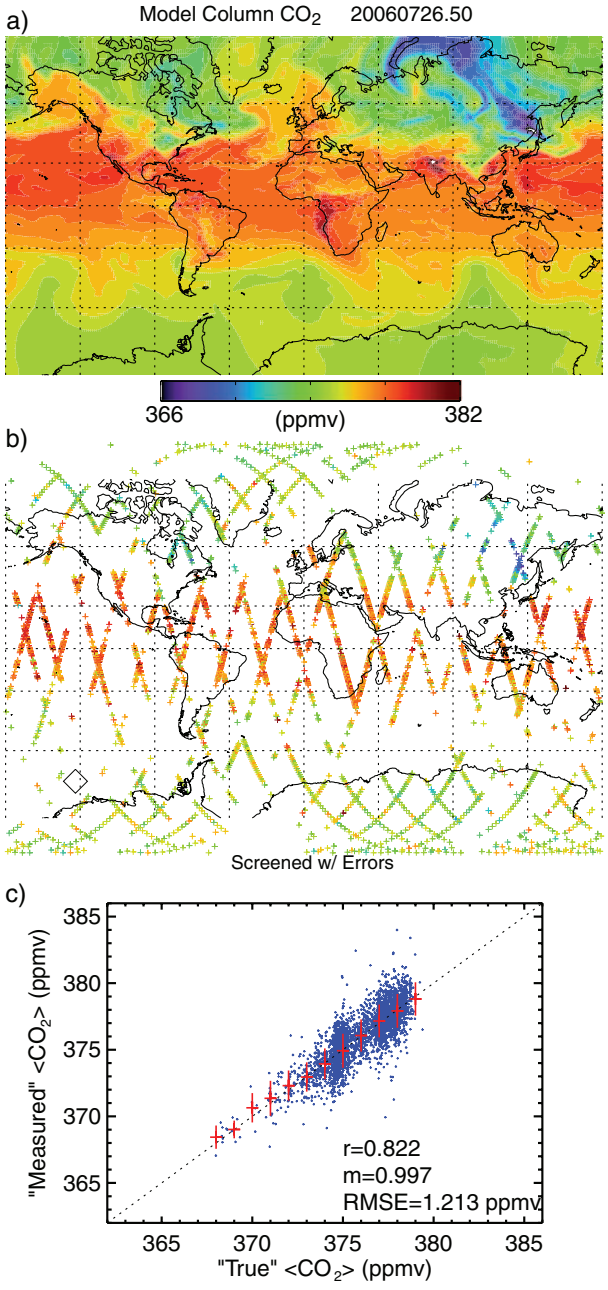

Fig. 4. Global synoptic field from the model on 2006-07-26 at 1200 UT showing instantaneous gradients and variability of $<CO_2>$ (a). Distribution of cloud-screened pseudo-data measurements for this day from CO_2 laser sounder mission concept (b). Note that the symbol size in (b) is not proportional to the laser sample area, which is currently specified at 70 m across track by 70 km along (10-s integration time). Panel (c) correlates pseudo 'measured' data with original 'true' model data as sampled in panel (b), blue points and fit coefficients. Red symbols show mean and ± standard deviation of 'measured' data in 1-ppmv bins set by the 'true' data.

northern hemisphere and tropics resulting from weather systems that transport air masses along and across surface flux gradients. In particular, low CO_2 downwind of regions with large vegetation uptake in summer is seen in the North. High CO_2 from fossil fuel emission is associated with population centres as well as biomass burning in the tropics. The sampled, cloud-screened, error-containing 'data' representation over the entire day is seen in Fig. 4(b). Comparison of the pseudo data with the original sampled values (Fig. 4c) shows errors as large as several ppmv locally, but the global RMS error is 1.21 ppmv. RMS errors for other days in July range from 1.12 to 1.30 ppmv. Sample days from December 2006 are also in the same range. This demonstrates that a space instrument designed to the specifications of Table 1 would be able to achieve the performance requirements of ASCENDS assuming no other significant unmodelled errors. Global $<CO_2>$ measurements at this level of precision are expected to significantly reduce the uncertainty in inferred surface fluxes of CO_2 (Rayner et al., 2002). Note also that, by way of consistency check, the magnitude of the $<CO_2>$ error is close to the root sum of squares of the errors enumerated in Section 5, which is to be expected for uncorrelated error sources.

8. Pseudo-data examples

Depending on the application, it is likely that some averaging or compositing of the data would be done to reduce random errors. Using example pseudodata we can begin to address questions of how to optimally aggregate the data for maximum information content and minimum error. Figure 5 shows the sampled pseudo data for 2006-07-26 averaged into $10^\circ \times 10^\circ$ latitude–longitude regions and the difference from the 'true' average in space and time for that day. Although there are many grid elements without sampling, the total RMS error is reduced globally to about 0.7 ppmv. The sample RMS error alone (i.e. 'perfect instrument' averages constructed by sampling and averaging the original field without any measurement error) is about 0.4 ppmv. Slightly smaller sample errors are found in Northern winter (December, not shown) cases (∼0.3 ppmv) when the global $<CO_2>$ gradients are smaller.

All 'measured' samples from a 16-d orbit repeat cycle and the corresponding 16-d average model $<CO_2>$ field are shown in Fig. 6. Comparing the averaged full field to the instantaneous in Fig. 4, we see many details are smoothed by averaging the evolving field. The 'measured' field now, however, presents a fairly complete spatial representation. Spatial averaging of the 16-d accumulated data on varying grids is shown in Fig. 7. The total errors continue to decline with increasing averaging scale, although regional details of the $<CO_2>$ distribution are averaged out. Errors ('true'—'measured') are largest where they might be expected: in regions of large gradients that are evolving in time, for example Northern mid to high latitudes. The best way to use the 'data' will depend on the application. For example, some inverse model methods are limited to coarse observation

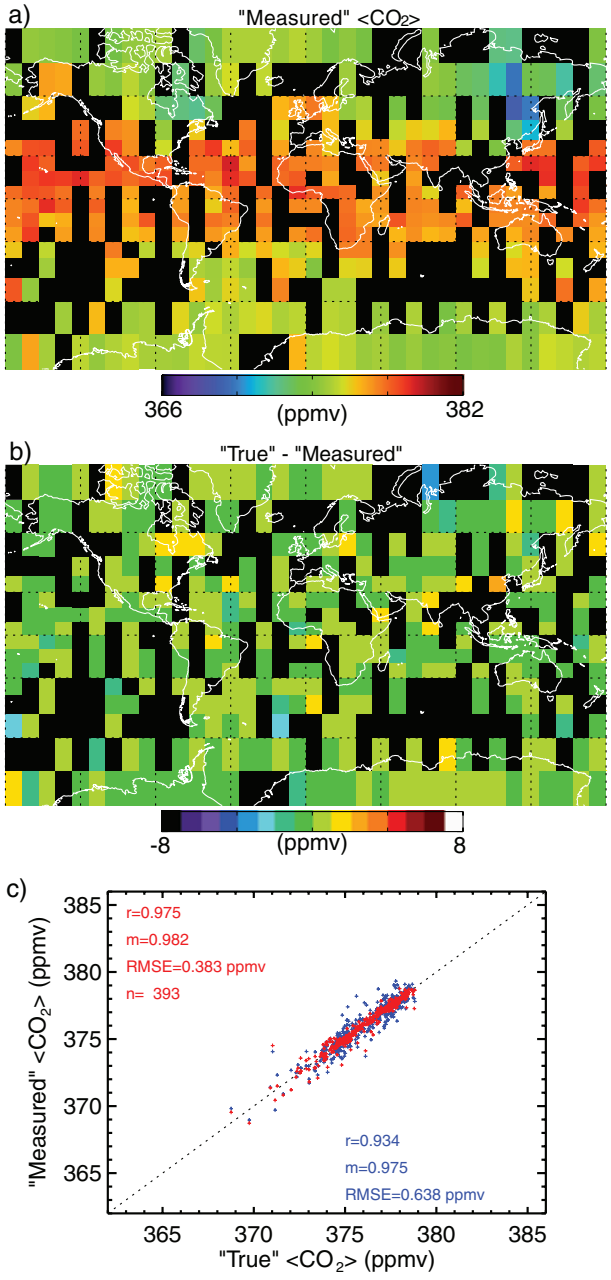

Fig. 5. $<CO_2>$ pseudo-data averaged into $10^\circ \times 10^\circ$ latitude/longitude grid boxes (a) and the difference of the 'measured' averages from the 'true' value in that grid box (b), which is formed by averaging all the model $1^\circ \times 1.25^\circ$ grid points in the box for that day (2006-07-26). Black grid areas contain no valid samples on this day. Panel (c) shows the correlation of 'true' versus 'measured' grid averaged samples and fit statistics for the full measurement errors (blue) and those due only to incomplete sampling of the model average (red).

grids by computational constraints, whereas other methods may be able to ingest individual soundings over several weeks or more. The pseudo data and errors that we have generated will be available for further analysis.

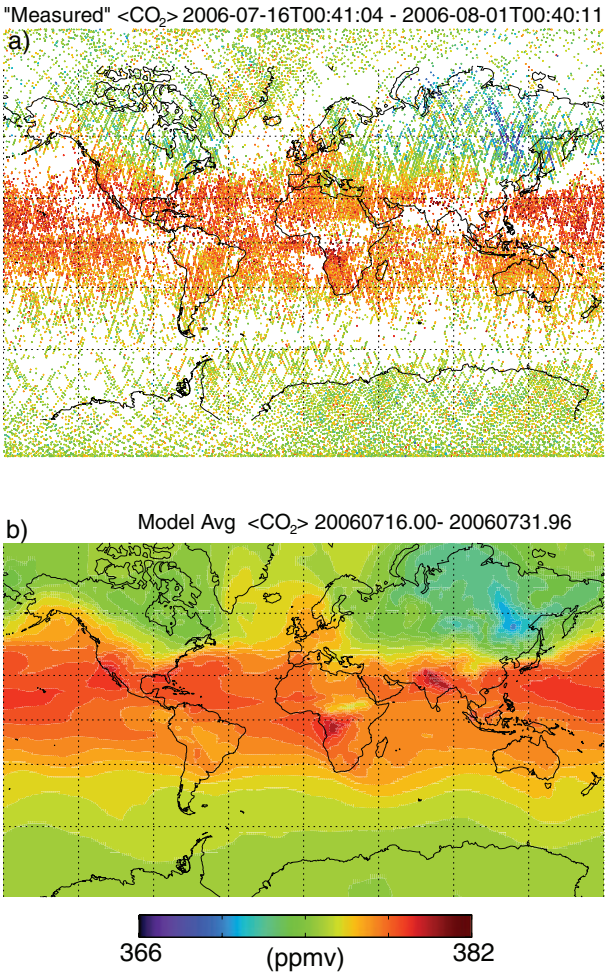

Fig. 6. One 16-d orbit repeat cycle of pseudo data (a) in July 2006 (symbols as in Fig. 4) and model time–average field over that interval (b). On two of the 16 d, CALIPSO sampling is limited to only a few orbits and other days are missing occasional orbits, but this somewhat reduced duty cycle may well be representative of the CO_2 laser sounder too. This time period was early in the CALIPSO mission, which began producing science data in June 2006. Most of the missing data areas (white regions), however, are a result of persistent cloud cover.

As a further test of data aggregation and sampling methods, we used a dawn/dusk orbit sampling rather than the near-midday/midnight orbit model of CALIPSO. The 'data' over the 16-d repeat cycle at approximately 0600 and 1800 local solar time are shown in Figs 8(a) and (b) using the same instrument model as earlier. Note that the individual sample errors are lower here than for the daytime samples above because the solar background radiance is small near dawn/dusk. The aggregate 16-d, 5-degree averaged difference between the dusk and dawn $<CO_2>$ fields is shown in Fig. 8(c). A 0600/1800 local time equator-crossing orbit was chosen because globally the maximum average 12-h $<CO_2>$ difference in the model occurs for these times. The full model ($1^\circ \times 1.25^\circ$) dusk–dawn (1800–0600

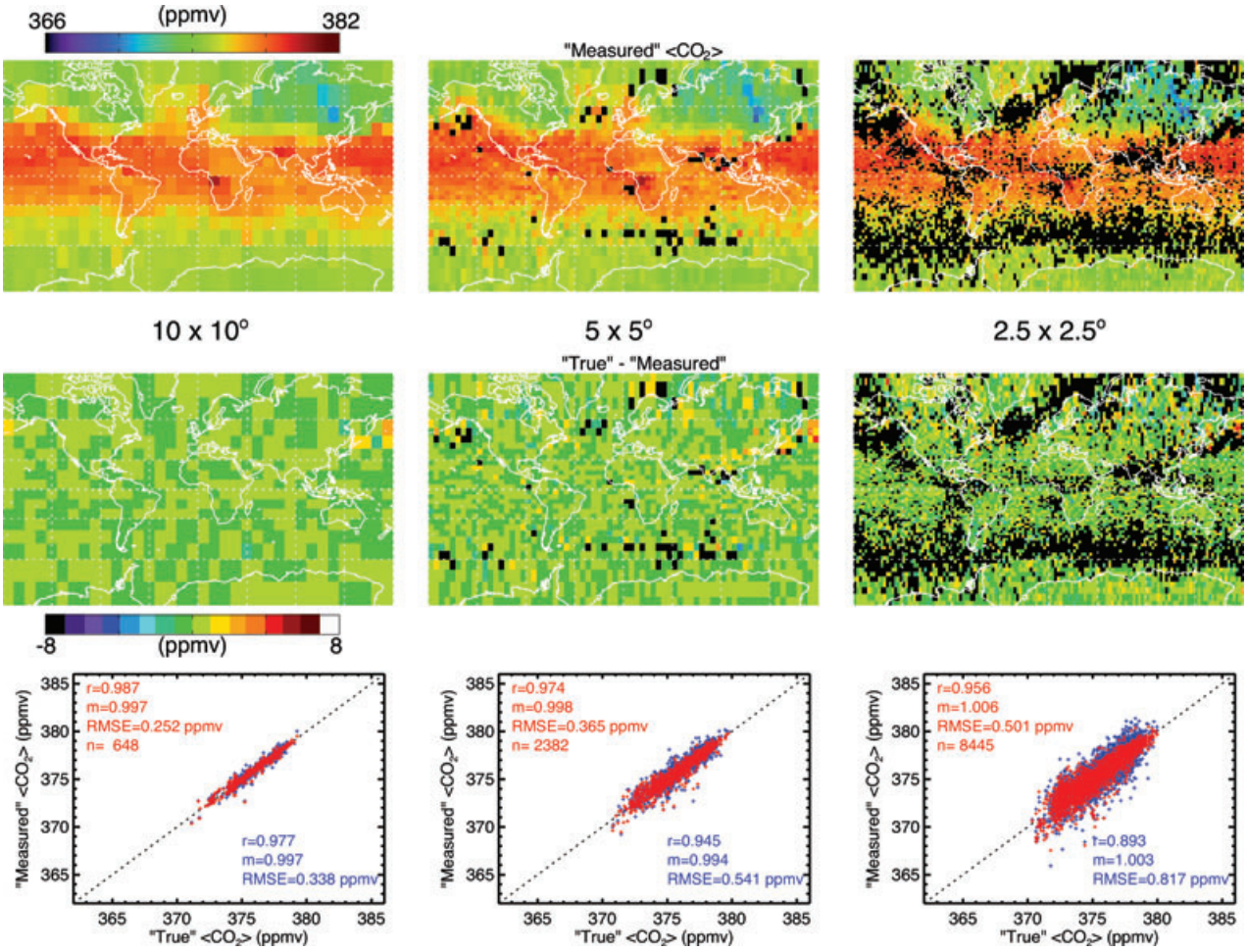

Fig. 7. Examples of the impact of spatial averaging grid on pseudo data from the 16-d repeat cycle shown in Fig. 6. Black grid areas contain no 'measured' samples. Error fields (second row) are differences of the averaged, sampled pseudo data from the corresponding full time/space resolution grid averages from the model. Correlation plots as in Fig. 5.

local solar time) difference averaged over 16 days (not shown) has maximum values for $<CO_2>$ of 0.5–1.5 ppmv over actively photosynthesizing vegetation, that is tropical forest in equatorial South America and Africa, and northern temperate and boreal forests in North America and Eurasia. Maximum differences are less than 1 ppmv when averaged up to 5° bins. Some semblance of this distribution can be seen in Fig. 8(c), but the errors (noise) are larger than the expected signal in most areas. The global RMS error in the 'true' versus 'measured' diurnal difference is 0.9 ppmv and the correlation coefficient (r) is about 0.3. Much of this error is due to sampling error (RMS = 0.6 ppmv) in trying to extract a diurnal difference from the relatively large, evolving synoptic $<CO_2>$ variations. Note, however, that measurements with a strong near-surface weighting function would likely improve detection of the diurnal difference more than proportionately because almost the entire signal arises from CO_2 change at the vegetation canopy level.

9. Summary and future applications

Simulation studies are presented for a laser-based CO_2 space mission that generally corresponds to the ASCENDS (NRC, 2007). CO_2 pseudo-data distributions and uncertainties are quantified using a realistic description of the atmosphere and surface state with a representative model of the instrument capabilities. This framework provides a comprehensive test bed to examine many potential implementation options and sensitivity to environmental conditions. Most of the expected major measurement error sources are included in detail (random radiance noise, surface pressure uncertainty, representation error, ground reflectance/wavelength shift error). Some additional potential error sources such as sub-grid scale variability will be explored further and incorporated when quantified. Also, more sophisticated multi-wavelength retrieval approaches will be included when available.

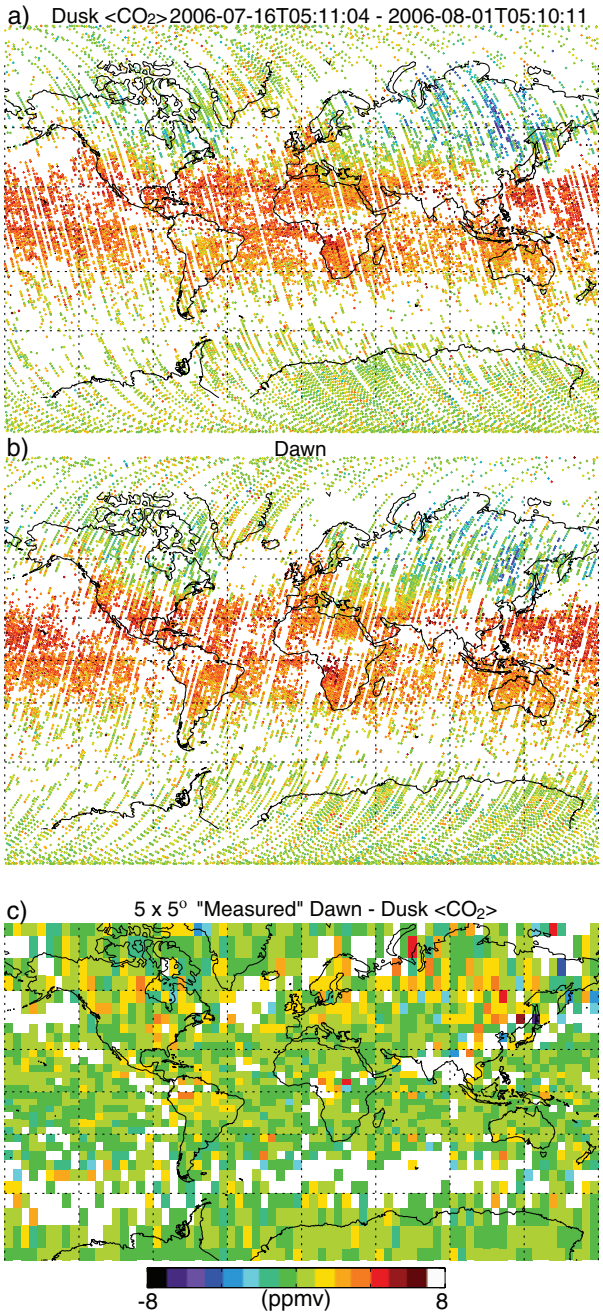

Fig. 8. Test of sampling from a near-dawn/dusk orbit (0600/1800 local solar time) for the 16-d repeat cycle of the CALIPSO orbit. Ascending (1800 hours) and descending (0600 hours) orbit node pseudo-data samples are shown separately in (a) and (b). Colour scale as in Fig. 6. The 5° grid-averaged difference between the dusk and dawn samples is shown in (c). White grid areas in (c) have no samples from either one or both nodes.

The error characteristics estimated for the CO_2 laser sounder's present design (i.e. orbit height, sample time, laser power, detector efficiency, etc.) indicate that such a mission can meet the ASCENDS measurement requirements and provide important new insights into carbon cycle science. Data precision on the order of 0.5% RMS appears possible with existing technologies on a single 10-s (70-km) sample basis. Random error reduction is quantified for several examples of space–time averaging.

Detecting perturbations in the diurnal balance between photosynthesis and respiration fluxes of CO_2 to inform the status and health of underlying vegetation will not be readily attainable from $<CO_2>$ measurements. This measurement requirement for ASCENDS (NRC, 2007) should be revisited in comparison to a midday/midnight orbit, which is near the time of the local daily mean $<CO_2>$ over vegetation, that is sampling is unbiased diurnally with respect to the mean (cf. Rayner et al., 2002).

An important next step will be to input the pseudo data into a CO_2 source/sink inversion model(s) and calculate the resulting uncertainty in regional to global surface flux estimates. Because flux results will depend on the specifics of the inverse model and methodology, perhaps several models will be used to compare between inverse applications and among a targeted set of mission options. Meanwhile, there is much that can be learned from further application of our framework with the forward model. We plan to fill out an annual cycle of pseudo data to determine measurement precisions for the global distribution of the CO_2 seasonal cycle, which provides a powerful constraint on our representation of source/sink processes and their response to environmental forcing. In addition, we can quantitatively test mission, instrument and retrieval approaches for their ability to measure CO_2 and address key carbon science hypotheses.

10. Acknowledgments

We acknowledge the support of the NASA Earth Science Technology Office's Advanced Instrument Technology and Instrument Incubator Programs, the NASA Carbon Cycle Science Program and Goddard Internal Research and Development. CALIPSO data were obtained from the NASA Langley Research Center Atmospheric Science Data Center and MODIS data were obtained from the Land Processes Distributed Active Archive Center (LP DAAC).

References

Abshire, J. B., Riris, H., Sun, X., Krainak, M. A., Kawa, S. R. and co-authors. 2007. Lidar approach for measuring the CO_2 concentrations in the troposphere from space. In: *Proceedings of 2007 Conference on Lasers and Electro-Optics (CLEO-2007),* Baltimore, MD, *Paper CThII5, ISBN: 978-1-55752-834-6*.

Abshire, J. B., Riris, H., Hasselbrack, B., Allan, G., Weaver, C. and co-authors. 2009. Airborne measurements of CO_2 column absorption using a pulsed wavelength-scanned laser sounder instrument. In: *Proceedings of 2009 Conference on Lasers and Electro-Optics (CLEO-2009),* Baltimore, MD, *Paper CFU-2, ISBN: 978–1-55752–869-8.*

Amediek, A., Fix, A., Ehret, G., Caron, J. and Durand, Y. 2009. Airborne lidar reflectance measurements at 1.57 μm in support of the

A-SCOPE mission for atmospheric CO_2. *Atmos. Meas. Tech. Discuss.* **2**, 1487–1536.

Bian, H., Kawa, S. R., Chin, M., Pawson, S., Zhu, Z. and co-authors. 2006. A test of sensitivity to convective transport in a global atmospheric CO_2 simulation. *Tellus* **58B**, 463–475.

Baker, D. F., Law, R. M., Gurney, K. R., Rayner, P., Peylin, P. and co-authors. 2006. TransCom 3 inversion intercomparison: impact of transport model errors on the interannual variability of regional CO_2 fluxes, 1988–2003. *Global Biogeochem. Cycles* **20**, GB1002, doi:10.1029/2004GB002439.

Bousquet, P., Peylin, P., Ciais, P., Le Quere, C., Friedlingstein, P. and co-authors. 2000. Regional changes in carbon dioxide fluxes of land and oceans since 1980. *Science* **290**, 1342–1346.

Chevallier, F., Maksyutov, S., Bousquet, P., Breon, F.-M., Saito, R. and co-authors. 2009. On the accuracy of the CO_2 surface fluxes to be estimated from the GOSAT observations. *Geophys. Res. Lett.* **36**, L19807, doi:10.1029/2009GL040108.

Clough, S.A. and Iacono, M. J. 1995. Line-by-line calculations of atmospheric fluxes and cooling rates. 2: Applications to carbon dioxide, ozone, methane, nitrous oxide, and the halocarbons. *J. Geophys. Res.* **100**,16519–16535.

Clough, S.A., Iacono, M. J. and Moncet, J. L. 1992. Line-by-line calculation of atmospheric fluxes and cooling rates: application to water vapor. *J. Geophys. Res.* **97**, 15761–15785.

Corbin, K. D., Denning, A. S., Lu, L., Wang, J.-W. and Baker, I. T. 2008. Possible representation errors in inversions of satellite CO_2 retrievals. *J. Geophys. Res.* **113**, D02301, doi:10.1029/2007JD008716.

Cox, P. M., Betts, R. A., Jones, C. D., Spall, S. A. and Totterdel, I. J. 2000. Acceleration of global warming due to carbon-cycle feedbacks in a coupled climate model. *Nature* **408**, 184–187.

Crisp, D., Atlas, R. M., Breon, F.-M., Brown, L. R., Burrows, J. P. and co-authors. 2004. The orbiting carbon observatory (OCO) mission. *Adv. Space Res.* **34**(4), 700–709.

Disney, M. I., Lewis, P. E., Bouvet, M., Prieto-Blanco, A. and Hancock, S. 2009. Quantifying surface reflectivity for spaceborne lidar via two independent methods. *IEEE Transact. Geosci. Remote Sens.* **47**, 3262–3271.

Dobbs, M., Gypson, M., Neff, B., Pruit, J., Zimmermann, J. and co-authors. 2002. Validation of design for space based Tunable Diode Laser Absorption Spectroscopy payload. *Proc. SPIE* **4817**, 123–128.

Dufour, E. and Breon, F.-M. 2003. Spaceborne estimate of atmospheric CO_2 column by use of the differential absorption method: error analysis. *Appl. Opt.* **42**, 3595–3609.

Dufresne, J.-L., Friedlingstein, P., Berthelot, M., Bopp, L., Ciais, P. and co-authors. 2002. On the magnitude of positive feedback between future climate change and the carbon cycle. *Geophys. Res. Lett.* **29**, 1405, doi:10.1029/2001GL013777.

Ehret, G., Kiemle, C., Wirth, M., Amediek, A. Fix, A. and co-authors. 2008. Space-borne remote sensing of CO_2, CH_4, and N_2O by integrated path differential absorption lidar: a sensitivity analysis. *Appl. Phys. B* **90**, 593–608, doi:10.1007/s00340-007-2892-3.

Friedlingstein, P., Cox, P., Betts, R., Bopp, L., von Bloh, W. and co-authors. 2006. Climate-carbon cycle feedback analysis: results from the (CMIP)-M-4 model intercomparison. *J. Clim.* **19**, 3337–3353.

Gibert, F., Flamant, P. H., Bruneau, D. and Loth, C. 2006. Two-micrometer heterodyne differential absorption lidar measurements of the atmospheric CO_2 mixing ratio in the boundary layer. *Appl. Opt.* **45**, 4448–4458.

Gurney, K. R., Law, R. M., Denning, A. S., Rayner, P. J., Baker, D. and co-authors. 2002. Towards robust regional estimates of CO_2 sources and sinks using atmospheric transport models. *Nature* **415**, 626–630.

Intergovernmental Panel on Climate Change (IPCC), Climate Change. 2007. The physical science basis. In: *Contribution of Working Group I to the Fourth Assessment Report of the Intergovernmental Panel on Climate Change*. Cambridge University Press, Cambridge, UK and New York, NY, USA, 9996.

Kameyama, S., Imaki, M., Hirano, Y., Ueno, S., Kawakami, S. and co-authors. 2009. Development of 1.6 mu m continuous-wave modulation hard-target differential absorption lidar system for CO_2 sensing. *Opt. Lett.* **34**, 1513–1515.

Kawa, S. R., Erickson, D. J. III, Pawson, S. and Zhu, Z. 2004. Global CO_2 transport simulations using meteorological data from the NASA data assimilation system. *J. Geophys. Res.* **109**, D18312, doi:10.1029/2004JD004554.

Koch, G. J., Barnes, B. W., Petros, M., Beyon, J. Y., Amzajerdian, F. and co-authors. 2004. Coherent differential absorption lidar measurements of CO_2. *Appl. Opt.* **43**, 5092–5099.

Lancaster, R. S., Spinhirne, J. D. and Palm, S. P. 2005. Laser pulse reflectance of the ocean surface from the GLAS satellite lidar. *Geophys. Res. Lett.* **32**, L22S10, doi:10.1029/2005GL023732.

Langenfelds, R. L., Francey, R. J., Pak, B. C., Steele, L. P., Lloyd, J. and co-authors. 2002. Interannual growth rate variations of atmospheric CO_2 and its delta C-13, H-2, CH4, and CO between 1992 and 1999 linked to biomass burning. *Global Biogeochem. Cycles* **16**(3), Art. No. 1048, doi:10.1029/2001GB001466.

Law, R. M., Peters, W., Rodenbeck, C., Aulagnier, C., Baker, I. and co-authors. 2008. TransCom model simulations of hourly atmospheric CO_2: Experimental overview and diurnal cycle results for 2002. *Global Biogeochem. Cycles* **22**, GB3009, doi:10.1029/2007GB003050.

Mao, J. and Kawa, S. R. 2004. Sensitivity studies for space-based measurement of atmospheric total column carbon dioxide using reflected sunlight. *Appl. Opt.* **43**, 914– 927.

Menzies, R. T. and Tratt, D. M. 2003. Differential laser absorption spectrometry for global profiling of tropospheric carbon dioxide: selection of optimum sounding frequencies for high-precision measurements. *Appl. Opt.* **42**, 6569–6577.

Miller, C. E., Crisp, D., DeCola, P. L., Olsen, S. C., Randerson, J. T. and co-authors. 2007. Precision requirements for space-based X CO_2 data. *J. Geophys. Res.* **112**, D10314, doi:10.1029/2006JD007659.

Nemani, R. R., Keeling, C. D., Hashimoto, H., Jolly, W. M., Piper, S. C. and co-authors. 2003. Climate-driven increases in global terrestrial net primary production from 1982 to 1999. *Science* **300**, 1560–1563, doi:10.1126/science.1082750.

NRC. 2007. *Earth Science and Applications from Space: National Imperatives for the Next Decade and Beyond*. The National Academies Press, Washington, DC.

Olsen, S. C. and Randerson, J. T. 2004. Differences between surface and column atmospheric CO_2 and implications for carbon cycle research. *J. Geophys. Res.* **109**, D02301, doi:10.1029/2003JD003968.

Parazoo, N. C., Denning, A. S., Kawa, S. R., Corbin, K. D., Lokupitiya, R. S. and co-authors. 2008. Mechanisms for synoptic variations of atmospheric CO_2 in North America, South America and Europe. *Atmos. Chem. Phys.* **8**, 7239–7254.

Rayner, P. J. and O'Brien, D. M. 2001. The utility of remotely sensed CO_2 concentration data in surface source inversions. *Geophys. Res. Lett.* **28**, 175–178.

Rayner, P. J., Law, R. M., O'Brien, D. M., Butler, T. M. and Dilley, A. C. 2002. Global observations of the carbon budget. 3. Initial assessment of the impact of satellite orbit, scan geometry, and cloud on measuring CO_2 from space. *J. Geophys. Res.* **107**(D21), 4557, doi:10.1029/2001JD000618.

Rothman, L. S., Gordon, I. E., Barbe, A., Benner, D. C., Bernath, P. F. and co-authors. 2009. The HITRAN 2008 molecular spectroscopic database. *J. Quantit. Spectrosc. Radiat. Transfer* **110**, 533–572, ISSN 0022-4073, doi:10.1016/j.jqsrt.2009.02.013.

Schaaf, C. B., Gao, F., Strahler, A. H., Lucht, W., Li, X. and co-authors. 2002. First operational BRDF, albedo and nadir reflectance products from MODIS. *Remote Sens. Environ.* **83**, 135–148.

SOCCR. 2007. The First State of the Carbon Cycle Report (SOCCR): The North American Carbon Budget and Implications for the Global Carbon Cycle, Synthesis and Assessment Product 2.2. *Report by the U.S. Climate Change Science Program and the Subcommittee on Global Change Research*, Asheville, NC.

Stephen, M. A., Mao, J., Abshire, J. B., Sun, X., Kawa, S. R. and co-authors. 2008. Oxygen spectroscopy laser sounding instrument for remote sensing of atmospheric pressure. In: *Proceedings of the 2008 IEEE Aerospace Conference*, Big Sky, MT, Volumes 1–9, 1541–1546.

Stephens, B. B., Gurney, K. R., Tans, P. P., Sweeney, C., Peters, W. and co-authors. 2007. Weak northern and strong tropical land carbon uptake from vertical profiles of atmospheric CO_2. *Science* **316**, 1732–1735.

Tans, P. P., Fung, I. Y. and Takahashi, T. 1990. Observational constraints on the global atmospheric CO_2 budget. *Science* **247**, 1431–1438.

Tucker C. J., Pinzon, J. E., Brown, M. E., Slayback, D. A., Pak, E. W. and co-authors. 2005. An extended AVHRR 8-km NDVI dataset compatible with MODIS and SPOT vegetation NDVI data. *Int. J. Remote Sens.* **26**, 4485–4498.

van Der Werf, G. R., Randerson, J. T., Giglio, L., Collatz, G. J. and Kasibhatla, P. S. 2006. Interannual variability in global biomass burning emission from 1997 to 2004. *Atmos. Chem. Phys.* **6**, 3423–3441. SRef-ID: 1680-7324/acp/2006-6-3423.

Warren, S. G. 1982. Optical properties of snow. *Rev. Geophys.* **20**(1), 67–89.

Warren, S. G. 1984. Optical constants of ice from the ultraviolet to the microwave. *Appl. Opt.* **23**, 1206–1225.

Winker, D. M., Hunt, W. H. and McGill, M. J. 2007. Initial performance assessment of CALIOP. *Geophys. Res. Lett.* **34**, L19803, doi:10.1029/2007GL030135.

Yokota, T., Oguma, H., Morino, I., Higurashi, A., Aoki, T. and co-authors. 2004. Test measurements by a BBM of the nadir-looking SWIR FTS aboard GOSAT to monitor CO_2 column density from space. *Proc. SPIE* **5652**, 182, doi:10.1117/12.578497.